Readout of Plastic Scintillators with Cooled Large-Area Avalanche Photodiodes

A. Mykulyak [a,b], M. Kapusta [a], U. Lynen [b], M. Moszyński [a], W.F.J. Müller [b], H. Orth [b], C. Schwarz [b], M. Szawlowski [c], W. Trautmann [b], A. Trzciński [a], D. Wolski [a], B. Zwiegliński [a,*]

[a] *The Andrzej Soltan Institute for Nuclear Studies, PL-00681 Warsaw, Hoża 69, Poland*

[b] *Gesellschaft für Schwerionenforschung, D-64291 Darmstadt, Planckstrasse 1, Germany*

[c] *Advanced Photonix Inc., 1240 Avenida Acaso, Camarillo CA93012, USA*

Abstract

Time-of-flight measurements in multifragmentation of heavy, relativistic projectiles require very good time resolution and at the same time the detecting system must cope with a dynamic range of up to 8000:1. We look into the possibility of application of large-area avalanche photodiodes (LAAPDs) as alternative light sensors to meet the above requirements. The paper presents the results of our amplitude and time response studies of a plastic scintillator BC-408 readout with a ϕ16 mm LAAPD using radioactive sources. The measurements were performed using two different setups. The best time resolution has been obtained by exploiting LAAPD cooling to increase its gain beyond that accessible at room temperature. We reach 610 ps (FWHM) at -26°C for the corresponding LAAPD gain of ≈900 and the ^{90}Sr/^{90}Y β-ray source. We hope to reach below the desired 400 ps with the latter setup at

the higher light levels available with multifragmentation products.

Key words: Multifragmentation of heavy relativistic projectiles, Fragment time-of-flight measurements with BC-408 plastic scintillators, Amplitude and time response of a BC-408+LAAPD combination, LAAPD gain increase by its cooling, Limiting time resolution

1 Introduction

A specific difficulty encountered in ToF measurements in multifragmentation of heavy relativistic projectiles, such as Au ($Z_{\rm proj}$=79) or U ($Z_{\rm proj}$=92), is related to the rich spectrum of fragments ranging from protons up or close to the initial projectile. Since energy-loss is proportional to Z^2, the dynamic range of energy-losses encountered in a scintillator, for example, in U multifragamentation is of the order of 8000.

The present work has been motivated by the intention to study the applicability of large-area avalanche photodiodes (LAAPDs) as alternative light sensors to replace photomultipliers (PMTs) for multifragmentation. Avalanche photodiodes (APDs) are known to possess an order of magnitude wider dynamic range of linear operation than PMTs because of strong internal electric fields acting on the charged carriers in the region of p-n junction, where their avalanche multiplication occurs. An additional advantage of APDs, their being immune to high magnetic fields, is without relevance for the considered application, since the ToF-wall is usually [1,2] installed at the distance of sev-

* Corresponding author. Tel.: +(48) 22 5532138, fax: +(48) 22 6213829.
Email address: bzw@fuw.edu.pl (B. Zwiegliński).

eral meters from the magnet (see Fig. 1 from Ref. [1]), where the influence of a weak stray field on PMTs can easily be eliminated with the aid of μ-metal shielding.

The necessary prerequisite for implementing APDs as alternatives to PMTs is the demonstration that they can offer a comparable or superior timing performance. Fig. 2 (lowest panel) presents time resolution as a function of the fragment Z-value obtained with PMTs in Au+Au multifragmentation at 1 GeV/nucleon in the range $2 \leq Z \leq 79$ [3]. Since protons are also considered of interest in multifragmentation, we set our applicability criterion at Δt=400 ps for Z=1, previously achieved for Z=2, as seen in the bottom panel of Fig. 2.

The time dispersion, $\sigma_{\rm time}$, is proportional [4,5] to the ratio of two factors:

$$\sigma_{\rm time} \sim \sigma_{\rm noise}/(dV/dt), \tag{1}$$

where $\sigma_{\rm noise}$ is the rms voltage noise and dV/dt is the signal slope at threshold of the timing discriminator. In view of the rather low gain of $\approx$300 of the applied APDs (see Sect. 2) in contrast to $\approx 10^6$ typical for PMTs, the ultimate time resolution that one might eventually achieve is an open question. In the present paper we address this question using radioactive sources and we describe measures taken to improve on both factors. Since we are interested in the intrinsic time resolution, we used small samples of 50 and 40 mm length of the same material as used in the ToF-wall. Measurements with 25 MeV protons are prepared.

2 APD selection criteria

Maximising the efficiency of conversion of scintillation light into a useful electrical signal was the chief criterion for selecting an APD for the above application. The maximum of fluorescence emission of BC-408 [1] is centered at about 430 nm in the blue domain of light spectrum. Consequently, we have looked for an APD with high quantum efficiency in the range of wavelengths overlapping the BC-408 emission spectrum. Advanced Photonix Inc. (API) APDs of the 70-74 series [6], having quantum efficiency reaching 80 % in the range 400-700 nm, have been found as suitable candidates. They are fabricated with three diameters of sensitive area: 5, 10 and 16 mm. The largest diameter type 630-70-74 has an active area of $\approx$2 cm^2, comparable to the cross section area of the scintillator, thus about 60% of the light emerging from its exit face can be intercepted and processed. For the reasons of high sensitivity and large area the LAAPD 630-70-74 has been selected for experiments. The working bias range at room temperature is typically 1760 - 1870 V, with a gain of $\approx$50 at the lower and $\approx$300 at the upper limit of the interval.

Hamamatsu's S8664-55 [2], widely renown for its application for $PbWO_4$ readout in the electromagnatic calorimeter of the CMS detector at CERN [7,8], has not been considered as a suitable candidate because of its small active area of 25 mm^2. However, an attractive feature of S8664-55 in any large scale application is its low operating voltage of about 400 V. We may modify our evaluation of APD applicability in favor of Hamamatsu, if their technology is

[1] Bicron, a division of Saint-Gobain Industrial Ceramics Inc., Scintillation Products, 12345 Kinsman Rd., Newbury OH 44065, USA; Website: www.bicron.com

[2] Hamamatsu Photonics; Website: www.hamamatsu.com

successfully extended towards larger area devices, which seem to be required at these lower light levels.

3 Electronics

Our electronics was a standard fast-slow coincidence system mostly based on ORTEC NIM modules. Start signals were derived from an XP2020 anode. In the APD branch the preamp time output has been further amplified with a variable gain 30 - 50 fast postamplifier, which was designed at SINS. The time signals were fed into ORTEC type 935 quad constant-fraction discriminator (CFD) and then into an ORTEC type 566 time-to-amplitude converter. Time calibration was performed using an ORTEC model 462 time calibrator. Employing a fast-slow coincidence system energy cuts could be set in both branches.

4 Measurements of light conversion efficiency and time resolution at room temperature

4.1 Number of e-h pairs/MeV electron energy deposited in BC-408

The number of e-h pairs per MeV electron energy deposited in the scintillator was derived from results of measurements of two spectra (see Fig. 3) following the procedure developed in [9]. The spectrum of ^{93}Mo X-ray source, shown in Fig. 3a, was used for calibration of the LAAPD. This spectrum was measured with a bare LAAPD 630-70-72-501, so that the Nb 16.6 keV K_α and 18.6 keV K_β X-rays are totally absorbed in its collection region. Fig. 3b shows the scin-

tillation spectrum from a sample of BC-408 of 50 mm length, installed with its 25×10 mm edge in optical contact with the APD window, illuminated at the opposite edge with a 662 keV ^{137}Cs γ-ray source. This produces a pure Compton spectrum in the organic material of BC-408, whose estimated edge position is indicated with an arrow in Fig. 3b together with the assigned energy. Note the amplifier gain decreased by a factor of 2 in 3a in comparison with 3b. From these two measurements we get 1520±50 e-h pairs/MeV electron energy deposited in BC-408 as an estimate of light conversion efficiency in our system scintillator-APD. Thus, one can estimate that a scintillator perfectly matching in size the APD area would produce 1520×25/16≈ 2380±80 e-h pairs/MeV. This latter number should be compared with 37000±1100 e-h pairs/MeV, quoted for CsI(Tl) [9], one of the most efficient scintillators, and 50 e-h pairs/MeV for $PbWO_4$ [8], one among the poorest γ-ray energy-to-light converters.

Our result partly reflects also the quality of light transport from its origin in the scintillator volume to the APD sensitive area. We have investigated different reflecting materials: aluminum foil, aluminized mylar and commercial teflon foil to select the one giving the best transmission, reflected by the highest position of the ^{137}Cs Compton edge. Three layers of a teflon tape are found the best among the three studied reflectors. The above result refers to this coating. In the three studied cases, the scintillator, after being wrapped with a reflector, was coupled with silicone oil to the APD glass window. Inserting a silicone rubber pad between the scintillator edge and the APD surface boosts the signal amplitude by 25%. This was possible to test with the windowless LAAPD used in Sect. 5.

4.2 Time resolution with ^{60}Co γ-ray source

In order to estimate time resolution attainable with the BC-408+LAAPD combination we performed measurements of time spectra of coincidences between ^{60}Co cascade γ-rays. One of the γ-rays was detected in a ϕ1" $\times$1" BaF_2 crystal coupled to a PMT XP2020Q, whose anode pulse provided the start signal for the TAC (see Sect. 3 for some additional details on the employed electronics). The stop signal was provided by the second γ-ray detected with the above mentioned 50 mm BC-408+LAAPD combination. This was installed directly on the preamp SHV connector and the bias voltage was 2472V with the corresponding LAAPD gain of 300. This voltage stands in an apparent conflict with the number quoted for 630-70-72 in Sect. 2, however, in this initial stage of the work, we used the older API products, typified by the operating range 2400-2500 V. The detectors looked face-to-face at each other with the ^{60}Co source inserted in between them. In order to check the time resolution of the BaF_2+PMT branch, we replaced our BC-408+LAAPD with another BaF_2 crystal coupled to XP2020Q, to get the FWHM of 140-150 ps, therefore we conclude that the time resolutions quoted below are mostly determined by the LAAPD branch.

Fig. 4 illustrates the effect of energy selection in the APD branch on time resolution obtained with the preamplifier ORTEC model 142AH. The solid line reveals three spectrum components: a uniform background of accidental coincidences, related to large extent with noise pulses from the APD, a broad maximum of the true coincidences between two pulses in which the constant fraction principle was not observed by one of the CFDs, and the topmost component containing events from the γ-quanta in the same cascade with

the CFDs working properly. This conclusion is based on a comparison of the solid and dashed lines in Fig. 4, the latter measured with a threshold set in the LAAPD slow channel, eliminating from the TAC spectrum the events provoked by small pulses, which results in an almost complete elimination of the second component.

Fig. 5a presents a similar set of data measured with the GSI CATSA preamp in the APD branch. The spectrum marked 0 in Fig.5a was taken without energy selection. The two coincidence spectra measured with energy selection, marked as 1 and 2 in Fig. 5a, had their thresholds as indicated with the vertical arrows marked 1 and 2, respectively, on Fig. 5b. Fig. 5b is the BC-408 Compton spectrum from the preamp energy output. The threshold at channel ≈75 in Fig. 5b was defined within the multichannel analyser and had no influence on amplitude selection for the time spectrum 0.

Besides some tailing towards higher amplitudes seen in the spectrum 0 on Fig. 5a, one can recognize here the same three-component structure and its variation with energy threshold as noted above in the discussion of Fig. 4. However, comparing the FWHMs 2.3 ns (Fig. 4) vs 1.2 ns (Fig. 5a), obtained under similar threshold settings with 142AH and CATSA, respectively, one notes a significant improvement in time resolution reached with the latter preamp. We conclude on the important role of preamp risetime in applications, as the present one, in which a fast scintillator (τ_{scint} =2.1 ns for BC-408) is read with a sensor of rather large capacitance ≈130 pF. The faster risetime given by CATSA permits also to reach a more complete compensation of amplitude-dependent time slewing around the triggering level of the CFD, a conclusion which follows from the observed difference 3.4 ns vs 1.4 ns between the widths measured without energy selection. This faster risetime we tend

to ascribe to the extraction of fast "loop error" signal (see e.g. [10]) from the collector of the input FET, further used as an output pulse for timing in CATSA. Moreover, both its fast rise and fall times make it possible to use a cheap fast DC amplifier, such as the one mentioned in Sect. 3 to drive CFD, liberating from the necessity to apply an extra shaping.

5 Measurements with cooled LAAPDs

Cooling of an APD has been previously profitably exploited to enhance the signal-to-noise ratio in minimum ionizing particle detection with submillimeter scintillating fibers [11,12]. An increase in gain by more than an order of magnitude has been observed in Ref. [11] upon cooling the APD from room temperature to -30°C. Gains of the order of 5000 are reached with LAAPDs at liquid-nitrogen temperatures [13,14]. These low temperatures are, however, beyond reach in the forseen LAAPD application (see Sect. 6). The mechanism of gain increase is ascribed [11] to a decreasing excitation of lattice vibrations (phonons) with the decreasing temperature of an APD silicon crystal. In an environment with fewer phonons the avalanche electrons can acquire higher energy, which tends to enhance the avalanche gain. We decided to employ this effect to enhance the signal slope in eq. (3) in order to improve time resolution attainable with the BC-408+LAAPD combination. These expectations are studied with the modified setup described in Sect. 5.1.

5.1 Experimental arrangement

In order to prevent the LAAPD sensitive surface from moisture deposition upon its cooling, the measurements were performed in a vacuum chamber, schematically presented in Fig. 6. The LAAPD is cooled using two thermoelectric modules (Peltier elements DT12-4 [3]) fixed between the two side copper plates and the central plate, which is silver-soldered in between the arms of a U-shaped, water-cooled copper tube, presenting a heat-sink for the "hot" sides of the Peltier elements. The side plates are in thermal contact with the Peltiers' "cold" sides, which provide cooling of the LAAPD-holder via flexible copper joints (cold-fingers). In order to improve thermal conductance in vacuum, the contacting surfaces are polished and covered with a thin layer of thermoconducting (but electroisolating) white paste P12 [4]. The temperature control is provided by Pt-100 resistive thermometers installed in two points: at the center of the right contact plate and on the LAAPD holder.

The BC-408 scintillator of 40 mm length is inserted between the cooled LAAPD housing and the front face of the PMT XP2020. We used a fresh batch of BC-408 to fabricate it. The plastic column of BC-408 provides a good thermal isolation from the PMT photocathode. The LAAPD shown is 630-70-74-510 (ϕ16 mm, windowless with a single-pin contact to the cathode, instead of an SHV connector). This pin is soldered with a thin covar wire to minimize heat leakage to the SHV male connector installed in the body of the chamber. The connector provides signal path to and HV from a preamp located outside the chamber. Our preference for a windowless LAAPD in these measurements was

[3] Marlow Industries, Inc., 10451 Vista Park Road, Dallas, TX 75238-1645, USA

[4] Wacker Chemie GmbH, Germany

motivated by an intention to test the effect of a contact medium between the LAAPD Si wafer and the exit face of BC-408 (see end of Sect. 4.1).

In the measurements reported below we turned to a ^{90}Sr/^{90}Y β-ray source whose end-point energy 2.28 MeV permits to come somewhat closer to light levels expected in the multifragmentation experiments (see Sect. 1). The source was located just above the scintillator near its center, as shown in Fig. 6, illuminating it approximately along the 25 mm long edge, so that approximately one half of the emitted photons is sent towards the LAAPD, while the same amount is transported by multiple reflections towards the PMT cathode to generate the start pulse in the time-resolution measurements.

5.2 LAAPD gain vs. LAAPD temperature

In these measurements we used the ^{90}Sr/^{90}Y β-ray source. The LAAPD temperature was varied by changing the supply voltage of the Peltier elements in steps and the spectra have been registered after temperature indicated by the LAAPD holder thermometer settled down following each change ($\approx$15-20 min). The initial room-temperature LAAPD gain was set equal 50 (HV=1670V). The measured spectra are superimposed on Fig. 7, each spectrum labeled with the corresponding temperature. The two-component structure due to the cascade of β-transitions ^{90}Sr$\rightarrow^{90}$Y and ^{90}Y$\rightarrow^{90}$Zr with end-points 0.546 and 2.284 MeV, respectively, is resolved and seen for the spectra taken at the lowest temperatures. LAAPD gains as a function of the LAAPD temperature, based on the extrapolated position of the spectrum end-point, main amplifier gain setting and the assumed gain at room temperature (supplied by the producer) are indicated in Fig. 8 with triangles. We reach a LAAPD gain as high as 900

at -26°C, which confirms the conclusions of Ref. [11]. Dots display the reduction of LAAPD reverse current observed in this range of temperatures. The ultimate low temperature reached is defined by the thermal pumping speed at the used maximum power rating of DT12-4s and by the thermal losses from the LAAPD housing to the elements which are in contact with it.

5.3 Time resolution

In these experiments only the CATSA preamp was used because of the better time resolution that can be expected (see Sect. 4.2). Figure 9 presents the spectra measured with the LAAPD cooled down to -26°C. In the upper panel (Fig. 9a) are shown the time spectra measured with (solid line) and without (dashed line) amplitude selection in the slow channels. There is a noteworthy qualitative change seen between the solid lines in Figs. 4, 5 as compared with the dashed line in Fig. 9a. What we have termed as the uniform background in Sect. 4.2 is virtually eliminated from the dashed curve in Fig. 9a, because all the coincidences are now real and the relative magnitude of the second component, corresponding to events poorly defined in time is also much reduced. Both FWHMs 820 and 610 ps, show a significant improvement in comparison with the results of Sect. 4.2. This improvement is due to a combination of several factors to mention at least two: higher electron energy used to excite BC-408 and higher LAAPD gain reached by its cooling. Figures 9b and 9c show the spectra as seen in the slow channels, the positions and widths of windows used to get the solid line in Fig. 9a are indicated. Comparing Fig.9b with 9c one concludes, that there is an identical perception of the ^{90}Sr/^{90}Y induced scintillations by both sensors.

6 Summary and outlook

Motivated by the intention of implementing APDs for light readout from plastic scintillators of the ALADIN ToF-wall in multifragmentation experiments, we have studied amplitude and time response of a BC-408+LAAPD combination with radioactive sources under different experimental conditions. A prerequisite for the foreseen application is achieving time resolution for protons not inferior than 400 ps (FWHM), observed at present for Z=2 with PMTs. We plan to verify whether this condition can be met with 25 MeV protons available from the compact cyclotron C-30 at SINS Swierk. This will be followed by an experiment at GSI, with full-length 110 cm scintillator rod(s) using fragmentation products of relativistic heavy-ion beams, in order to look into aspects related to dynamic range and time resolution for energetic fragments with $Z \geq$2.

The forseen application admits only a moderate LAAPD cooling to -20 - -30°C. Therefore, we used Peltier cooling modules and vacuum environment to perform these measurements. Our best result 610 psec obtained with the LAAPD at -26°C and the ^{90}Sr/^{90}Y β-ray source with energy selection (Sect. 5.3) is encouraging in that with higher light levels expected for fragments we hope to reach below the desired 400 psec.

The conclusions of the present work may find as well application in electromagnetic calorimeters utilizing APDs for light readout from $PbWO_4$ scintillators. Cooling the latter scintillator tends to increase its light output in this range of temperatures relative to that observed at room temperature [15,16]. This together with the improved performance of cooled LAAPD sensors may in-

crease the calorimeter sensitivity in the studies of charmed hadronic systems forseen, for example, with the future proton-antiproton (PANDA) facility at GSI [17]. LAAPD insensitivity to high magnetic fields is an essential feature for the latter application.

Acknowledgments

This work was supported in part by the European Community under contract ERBFMGECT950083 and by the BMBF (Bonn) - KBN (Warsaw) Collaborative Agreement in Science and Technology under contract POL-196-96.

References

[1] A. Schüttauf *et al.*, Nucl. Phys. A 607 (1996) 457.

[2] J.A. Hauger *et al.*, Phys. Rev. C 57 (1998) 764.

[3] A. Schüttauf, Untersuchung der Kernfragmentation, PhD Thesis, Institut für Kernphysik der Johann Wolfgang Goethe Universität, Frankfurt am Main, 1996 (unpublished).

[4] J.A. Hauger, Y. Choi, A.S. Hirsch, R.P. Scharenberg, B.C. Stringfellow, M.L. Tincknell, N.T. Porile, G. Rai, J. Garbarino, R.J. McIntyre, Nucl. Instr. and Meth. A337 (1994) 362.

[5] M. Moszynski, T. Ludziejewski, D. Wolski, W. Klamra, M. Szawlowski, M. Kapusta, IEEE Trans. on Nucl. Sci. 43 (1996) 1298.

[6] Advanced Photonix Inc. product description; avalanche photodiodes (LAAPDs), available at http://www.advancedphotonix.com

[7] K. Deiters, Q. Ingram, Y. Musienko, S. Nicol, P. Patel, D. Renker, S. Reukroft, R. Rusack, T. Sakhelashvili, J. Swain, P. Vikas, Nucl. Instr. and Meth. A 453 (2000) 223.

[8] J. Grahl, I. Kronqvist, R. Rusack, A. Singovski, A. Kuznetsov, A. Musienko, S. Reucroft, J. Swain, K. Deiters, Q. Ingram, D. Renker, T. Sakhelashvili, Proc. of the 10th Int. Conf. on Calorimetry in Part. Phys. Calor2002, 25-29 March 2002, Pasadena, California (USA), ed. by R.Y. Zhu, World Scientific, Singapore (2002), p. 231.

[9] M. Moszynski, M. Szawlowski, M. Kapusta, M. Balcerzyk, Nucl. Instr. and Meth. A 485 (2002) 504.

[10] J. Friese, A. Gillitzer, H.J. Körner, M.R. Maier, IEEE Trans. on Nucl. Sci. 40, 4 (1993) 339.

[11] T. Okusawa, Y. Sasayama, M. Yamasaki, T. Yoshida, Nucl. Instr. and Meth. A 440 (2000) 348.

[12] T. Okusawa, Y. Sasayama, M. Yamasaki, T. Yoshida, Nucl. Instr. and Meth. A 459 (2001) 440.

[13] M. Moszynski, W. Czarnacki, M. Szawlowski, B.L. Zhou, M. Kapusta, D. Wolski, P. Schotanus, IEEE Trans. Nucl. Sci. 49 (2002) 971.

[14] M. Moszynski, W. Czarnacki, W. Klamra, M. Szawlowski, P. Schotanus, M. Kapusta, Nucl. Instr. and Meth. A 504 (2003) 307.

[15] M. Kobayashi, M. Ishii, Y. Usuki, H. Yahagi, Proc. of the Int. Workshop Cristal 2000, Sept. 22-26, 2000, Chamonix (France), ed. by F. De Notaristefani, P. Lecoq and M. Schneegans, Editions Frontieres, Paris (1993), p. 375.

[16] W. van Loo, Phys. Stat. Sol. (a) 27 (1975) 565; ibid. 28 (1975) 227.

[17] An International Accelerator Facility for Research with Ions and Antiprotons, pp. 247-248 at http://www-new.gsi.de/GSI-Future/cdr.

Figure captions

Fig. 1. Section of the ALADIN facility [1] with a plane containing the central trajectory (dash-and-dot line). The dashed line represents the initial beam direction. The subsystems used in the experiment described in Ref. [1] are indicated.

Fig. 2. Charge (top), position (middle) and time (bottom) resolution of the ALADIN ToF-wall (PMT-readout) as a function of the detected fragment Z-value. Measurements have been performed using ^{197}Au+^{197}Au multifragmentation products at 1000 MeV/nucleon [1,3].

Fig. 3. (a) Spectrum of X-rays from the ^{93}Mo source taken with the same LAAPD as in (b) after removing the scintillator and keeping HV unaltered. Note the amplifier gain decreased by a factor of 2 in comparison with b. The energies of Nb K_α (16.6 keV) and K_β (18.6 keV) X-rays, corresponding to the observed peaks, are indicated. (b) Spectrum of Compton electrons from the ^{137}Cs γ-ray source in BC-408 readout with the LAAPD. The estimated position of the 460 keV Compton edge is indicated with an arrow.

Fig. 4. Time spectra of coincidences between the ^{60}Co γ-rays detected in the BaF_2 crystal coupled to a PMT XP2020Q and the BC-408 scintillator coupled to the LAAPD. ORTEC 142AH preamp has been used for the LAAPD signals. The solid line denotes the spectrum taken without energy selection. The dashed line is the spectrum taken with energy cut. FWHMs are marked with arrows and their values indicated.

Fig. 5. (a) Time spectra of coincidences between the ^{60}Co γ-rays detected

in the BaF_2 crystal coupled to a PMT XP2020Q and the BC-408 scintillator coupled to the LAAPD. CATSA preamp has been used for the LAAPD signals. The solid line (0) denotes the spectrum taken without energy selection. The dashed line (1) is the spectrum taken with the lower threshold setting shown in (b), while the dash-and-dot (2) line denotes the spectrum taken with the higher one. FWHMs are marked with arrows and their values indicated. (b) Amplitude spectrum of the Compton electrons created in BC-408 by the ^{60}Co γ-rays and readout with the LAAPD. Note the characteristic inflection point around the channel 640, reflecting a transition point between the two Compton edges. Arrows mark the positions of thresholds used in taking the dotted (lower threshold) and dash-and-dotted (higher threshold) spectra in (a).

Fig. 6. Vertical section of the vacuum chamber used for the measurements discussed in Sect. 5 showing its constituent elements: (1) LAAPD 630-70-74-510, (2) Plastic scintillator BC-408, (3) PMT XP2020, (4) Teflon plate, (5) LAAPD holder, (6) Flexible copper joint (cold-finger), (7) Side copper plates, (8) Central plate, (9) Water-cooled U-shaped copper tube, (10) Peltier elements DT12-4, (11) Vacuum feedthrough connecting to Pt-100 thermometers, (12) Vacuum feedthrough for power supply to DT12-4s, (13) Soft-iron housing of the PMT, (14) ^{90}Sr/^{90}Y β-ray source, (15) Pumping port to the chamber.

Fig. 7. Spectra of ^{90}Sr/^{90}Y β-particles from BC-408 readout with a cooled LAAPD at different temperatures (in deg C) indicated nearby the arrows.

Fig. 8. LAAPD gain (triangles) determined from the spectra of Fig. 7 and LAAPD reverse current (circles) as a function of the LAAPD temperature.

Fig. 9. (a) Time spectra of coincidences between the start signal derived from the anode of the PMT XP2020 and the stop signal derived from the LAAPD

cooled down to -26°C measured with (solid line) and without energy selection (dashed line) using the setup shown in Fig. 6. FWHMs of the spectra are indicated. (b) Amplitude spectrum from the CATSA energy output with the window selected for the solid line measurement in (a) indicated with the vertical arrows, (c) Amplitude spectrum from the XP2020 12-th dynode with the window selected for the solid line measurement in (a) indicated with the vertical arrows.

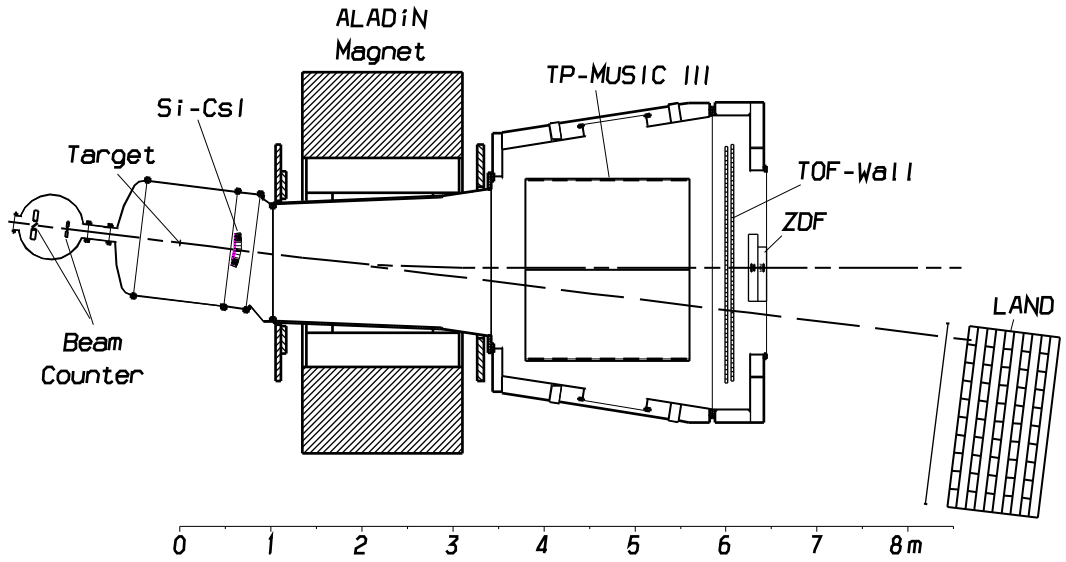
ALADiN
Magnet
TP-MUSIC III
Si-CsI
Target
TOF-Wall
ZDF
LAND
Beam
Counter
0
1
2
3
4
5
6
7
8 m

Fig. 1.

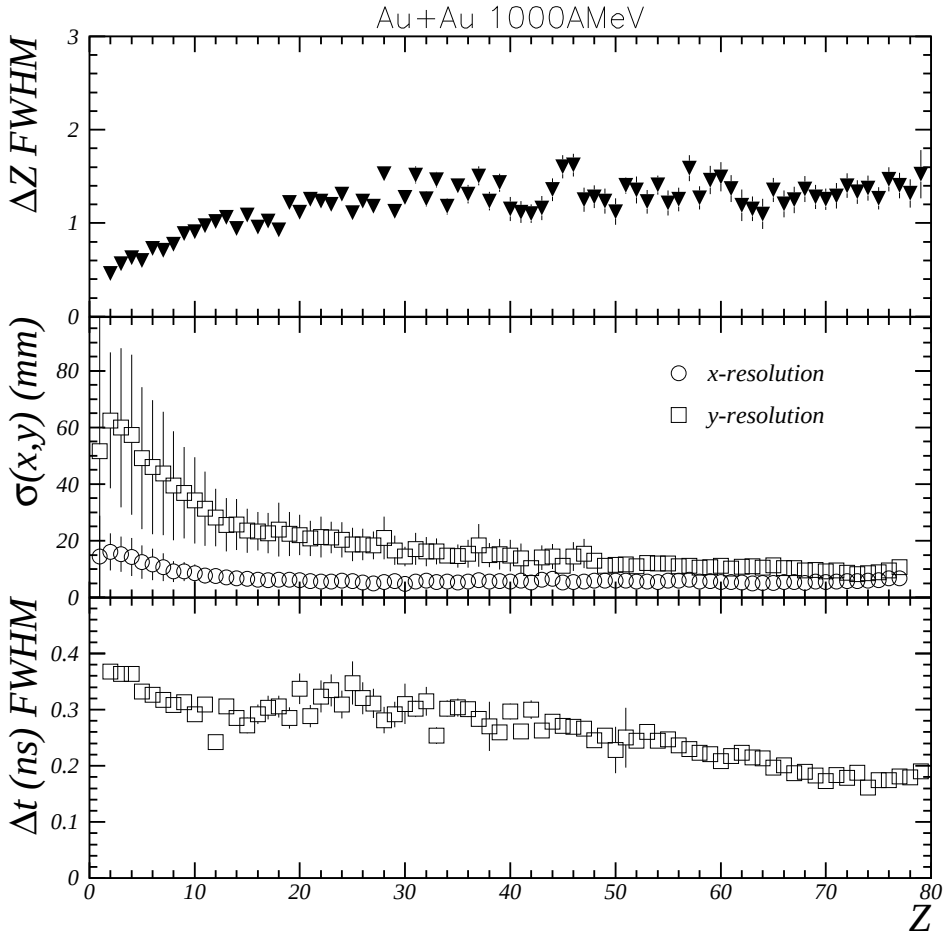
Au+Au 1000AMeV
ΔZ FWHM
σ(x,y) (mm)
x-resolution
y-resolution
Δt (ns) FWHM
Z

Fig. 2.

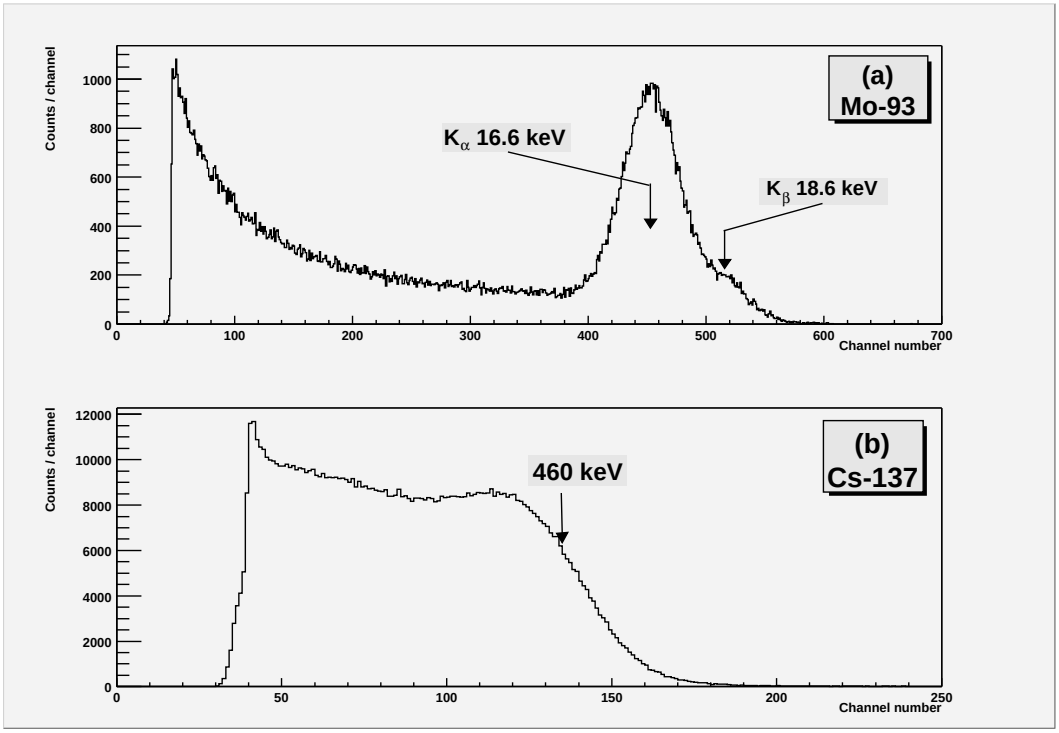
(a)
Mo-93
K_α 16.6 keV
K_β 18.6 keV
Counts / channel
Channel number
(b)
Cs-137
460 keV
Counts / channel
Channel number

Fig. 3.

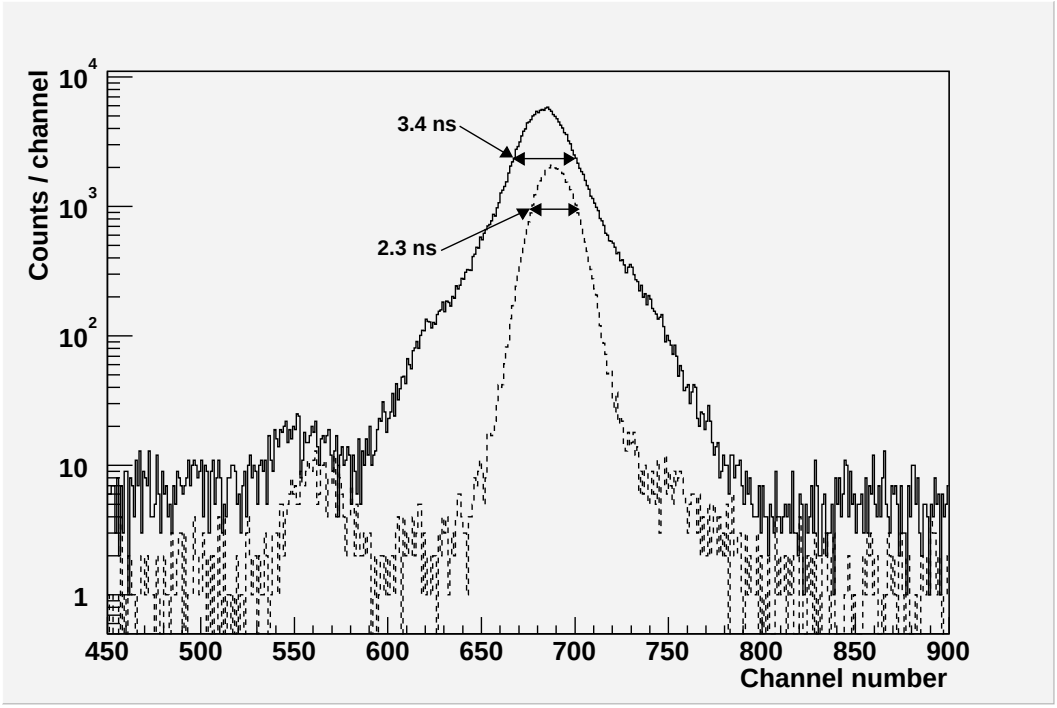
3.4 ns
2.3 ns
Counts / channel
Channel number

Fig. 4.

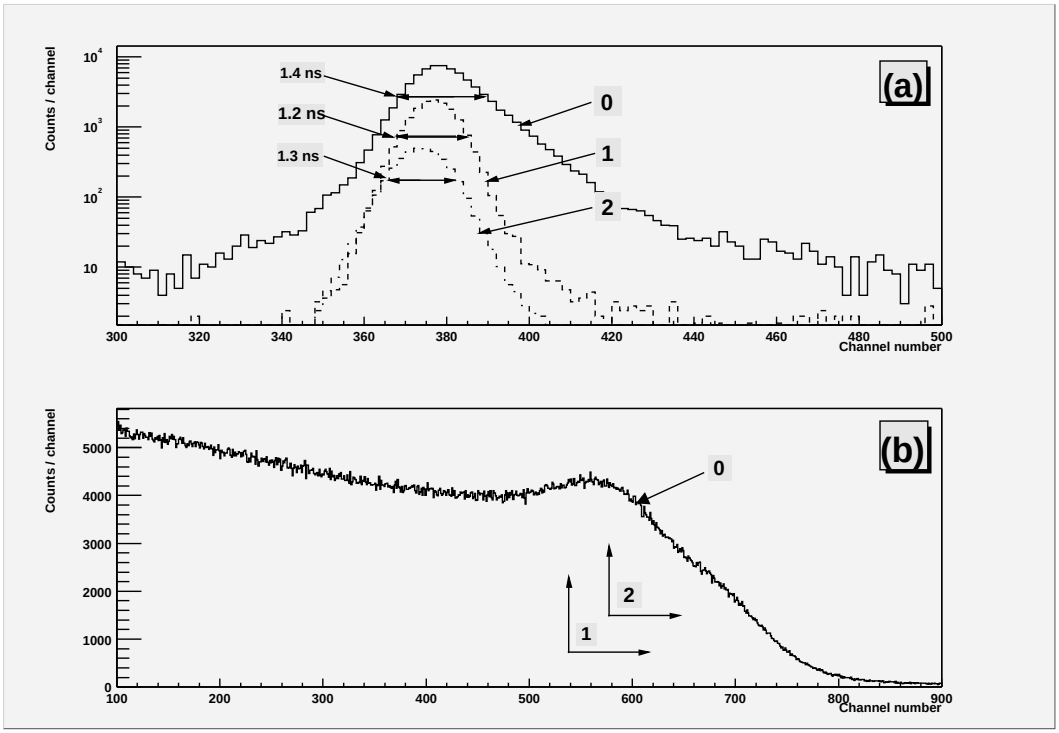
(a)
Counts / channel
1.4 ns
1.2 ns
1.3 ns
0
1
2
Channel number
(b)
Counts / channel
0
1
2
Channel number

Fig. 5.

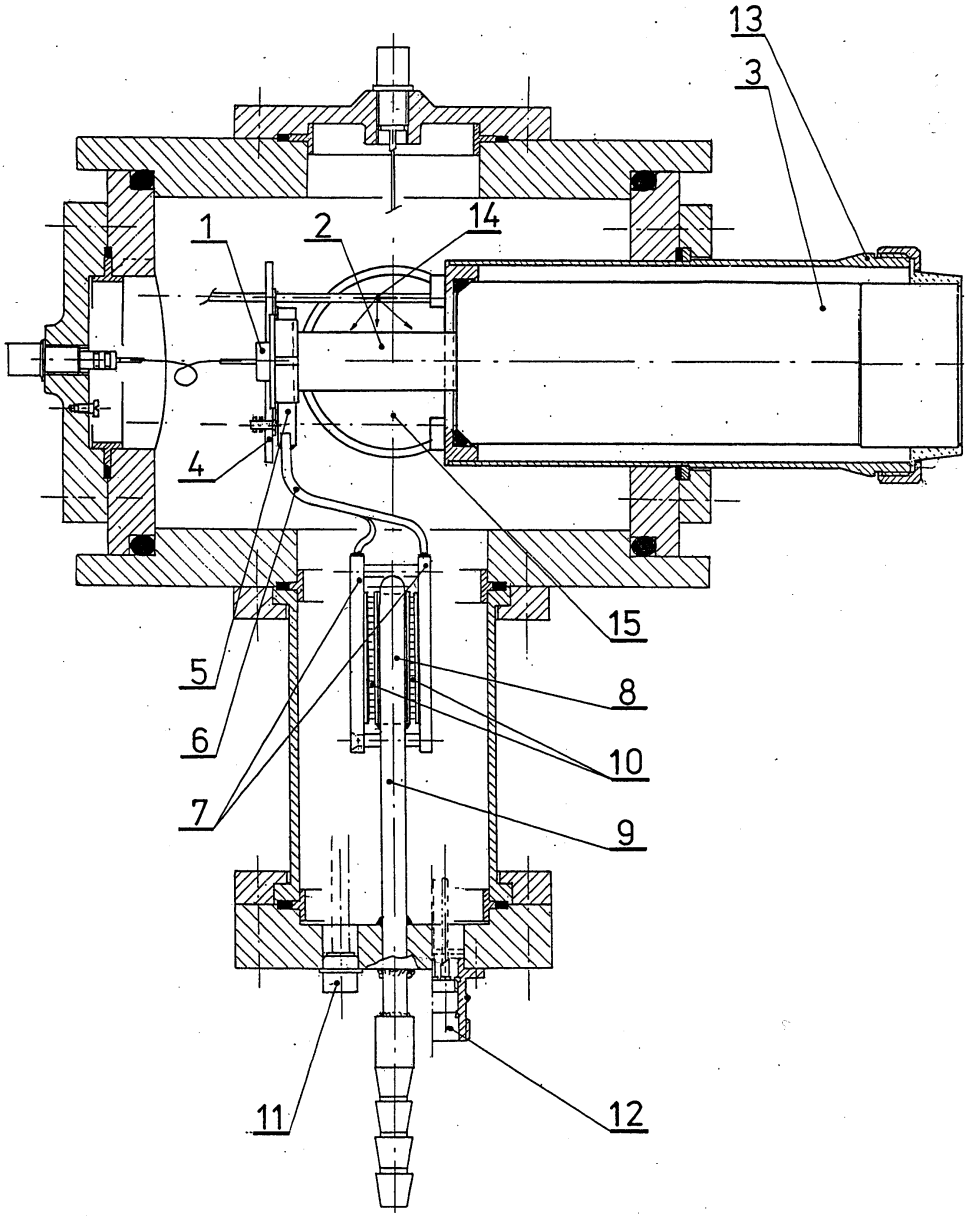

Fig. 6.

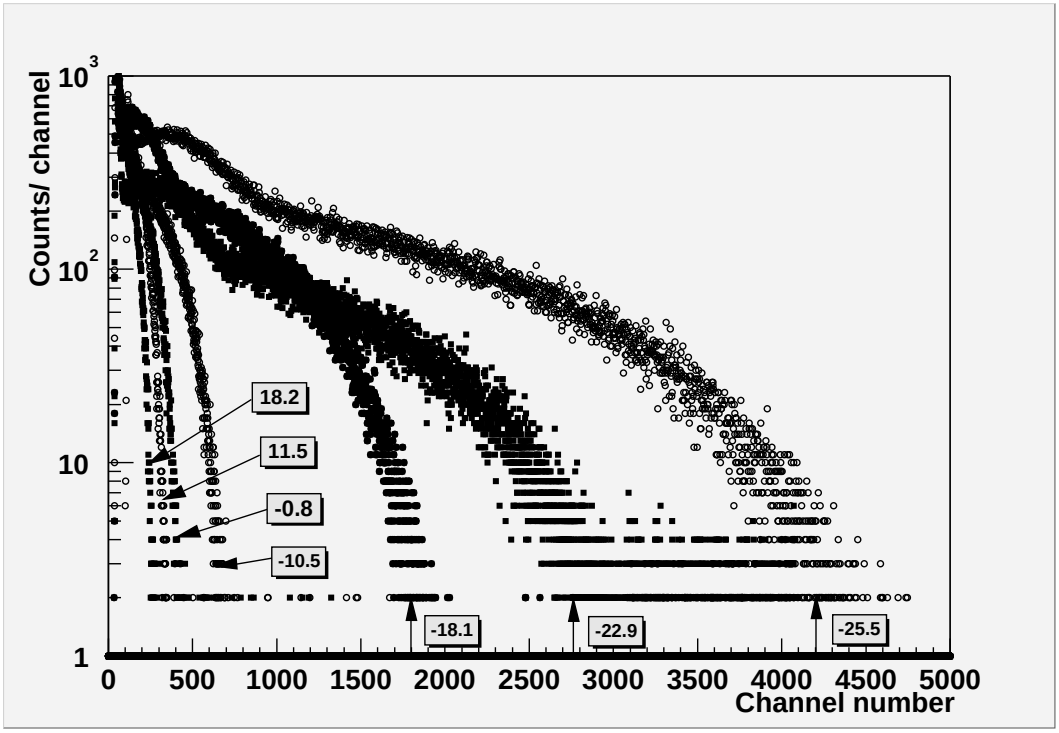
Counts/ channel
Channel number
18.2
11.5
-0.8
-10.5
-18.1
-22.9
-25.5

Fig. 7.

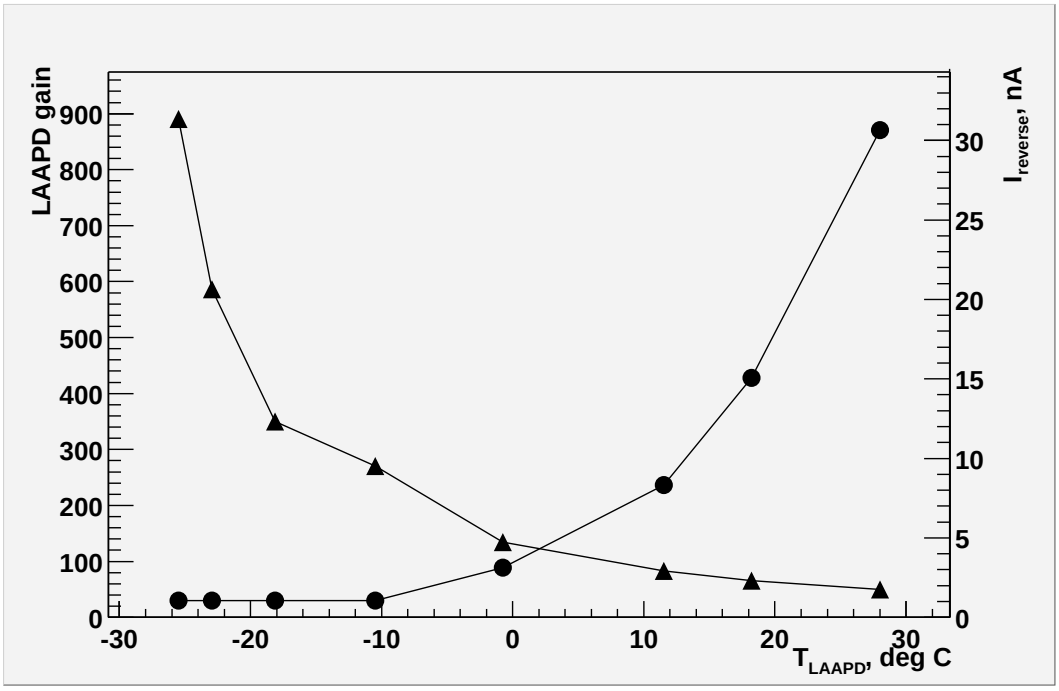
LAAPD gain
$I_{reverse}$, nA
T_{LAAPD}, deg C

Fig. 8.

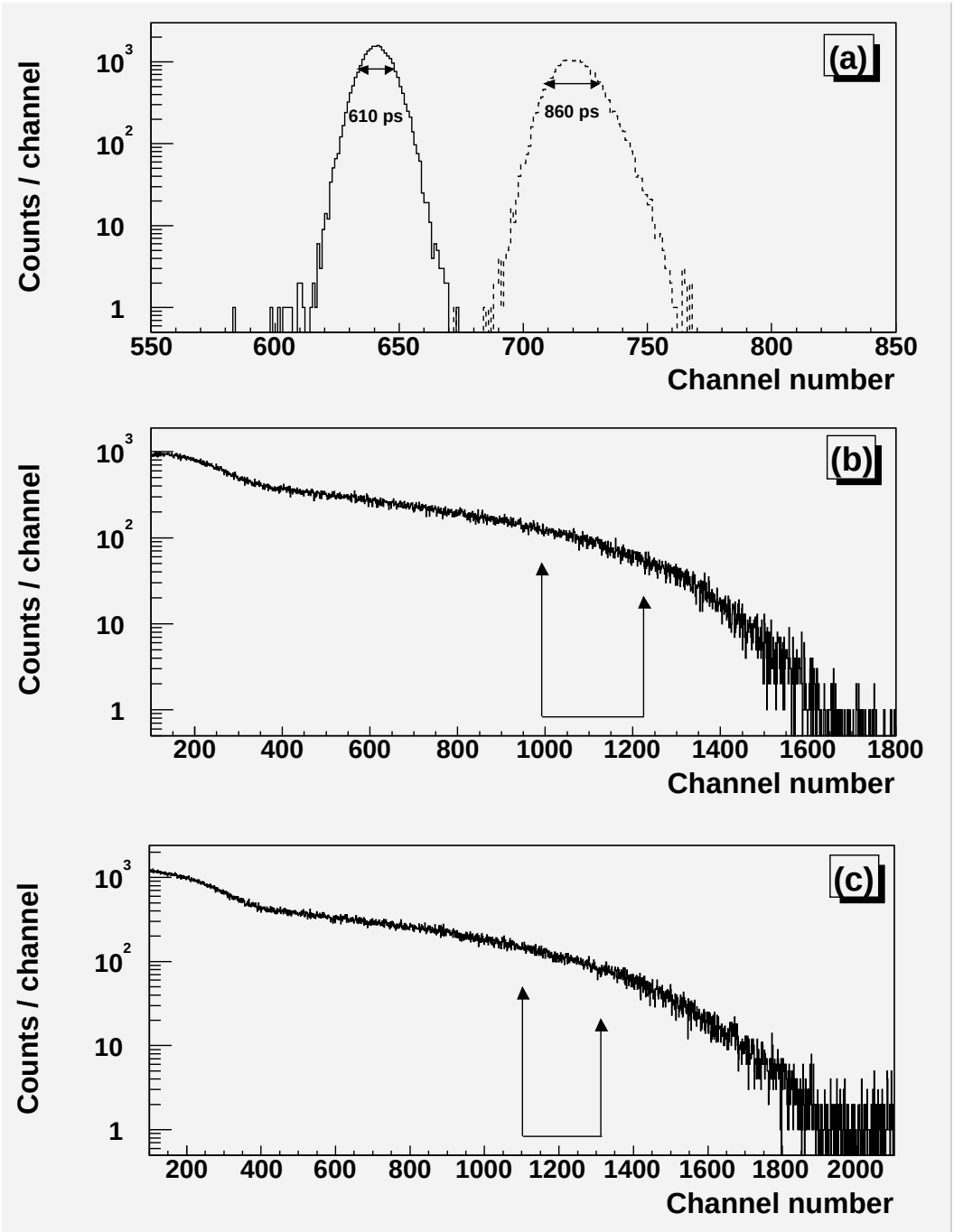
(a)
610 ps
860 ps
Counts / channel
Channel number
(b)
Counts / channel
Channel number
(c)
Counts / channel
Channel number

Fig. 9.